JCB Article

A biomimetic motility assay provides insight into the mechanism of actin-based motility

Sebastian Wiesner,[1] Emmanuele Helfer,[1] Dominique Didry,[1] Guylaine Ducouret,[2] Françoise Lafuma,[2] Marie-France Carlier,[1] and Dominique Pantaloni[1]

[1]Dynamique du cytosquelette, Laboratoire d'Enzymologie et Biochimie Structurales, Centre National de la Recherche Scientifique, 91198 Gif-sur-Yvette, France
[2]Physicochimie des Polymères et des Milieux Dispersés, UMR 7615, 75231 Paris cedex 05, France

A biomimetic motility assay is used to analyze the mechanism of force production by site-directed polymerization of actin. Polystyrene microspheres, functionalized in a controlled fashion by the N-WASP protein, the ubiquitous activator of Arp2/3 complex, undergo actin-based propulsion in a medium that consists of five pure proteins. We have analyzed the dependence of velocity on N-WASP surface density, on the concentration of capping protein, and on external force. Movement was not slowed down by increasing the diameter of the beads (0.2 to 3 μm) nor by increasing the viscosity of the medium by 10^5-fold. This important result shows that forces due to actin polymerization are balanced by internal forces due to transient attachment of filament ends at the surface. These forces are greater than the viscous drag. Using Alexa®488-labeled Arp2/3, we show that Arp2/3 is incorporated in the actin tail like G-actin by barbed end branching of filaments at the bead surface, not by side branching, and that filaments are more densely branched upon increasing gelsolin concentration. These data support models in which the rates of filament branching and capping control velocity, and autocatalytic branching of filament ends, rather than filament nucleation, occurs at the particle surface.

Introduction

Site-directed polymerization of actin filaments, in response to signaling, generates a force leading to cell protrusions called lamellipodia and filopodia (Mitchison and Cramer, 1996), or to the propulsion of pathogens like *Listeria* and *Shigella* (Cameron et al., 2000). Actin-based movement results from local sustained initiation of new filaments, whose steady polarized growth is fed by the ATP-consuming treadmilling of actin filaments (Pantaloni et al., 2001). Actin-based movement of *Listeria*, *Shigella* (Loisel et al., 1999), or any functionalized particle (Pantaloni et al., 2001; Wiesner et al., 2002) has been reconstituted in vitro from a minimum set of five pure proteins. The particle is coated with an activator of Arp2/3 complex, which is either a protein of the WASP family (Machesky and Insall, 1998) or the ActA protein of *Listeria* (Welch et al., 1998), which functionally mimics WASP (Skoble et al., 2000; Boujemaa-Paterski et al., 2001). The immobilized activator is an enzyme that makes a branching complex with one molecule of G-actin and Arp2/3 complex. This ternary complex associates with a filament to initiate the formation of a branch. Dissociation from the immobilized branching enzyme leads to two growing barbed ends from a single one. The details of the catalytic cycle of filament branching at a surface are not elucidated; however, it is clear that local multiplication of filament barbed ends by branching is a key event in the production of force and movement. In addition to actin, the motility medium contains regulatory proteins (actin-depolymerizing factor [ADF]*/cofilin, profilin, and a capping protein) that enhance the efficiency of treadmilling. Capping proteins cooperate with ADF to establish a high concentration of G-actin and, in arresting barbed end growth, control the life-time and average length of the filaments (Borisy and Svitkina, 2000; Pantaloni et al., 2000).

Although the general lines of the biochemical mechanism at the origin of actin-based motility are understood, important issues are open. Is velocity dependent on the number of pushing filaments? How is external load affecting velocity? What is the nature of the forces that control stationary pro-

The online version of this article includes supplemental material.

Address correspondence to Marie-France Carlier, CNRS, LEBS, Bât. 34, 1 Avenue de la Terrasse, F-91198 Gif-sur-Yvette, France. Tel.: 33-16-982-3465. Fax: 33-16-982-3129. E-mail: carlier@lebs.cnrs-gif.fr

Key words: actin; cell motility; N-WASP; Arp2/3 complex; biomimetics

*Abbreviations used in this paper: ADF, actin-depolymerizing factor; LTM, laser tracking microrheology.

pulsion? How is the molecular mechanism of Arp2/3 complex involved in movement? How is the density of filament branching determined in motility?

A chemically controlled motility assay can provide answers to these questions. Microspheres, functionalized in a controlled fashion, are a physiologically relevant model to analyze how the surface density of an activator of Arp2/3 complex affects motility and the morphology of the actin meshwork. In an initial study, microspheres derivatized with the *Listeria* protein ActA underwent actin-based movement in *Xenopus* egg extracts (Cameron et al., 1999, 2001; Noireaux et al., 2000) only when the bead diameter was <0.5 μm. In contrast, in the reconstituted medium, motility can be monitored in a broader diameter range than in cell extracts, typically from 0.2 to 10 μm (Pantaloni et al., 2001; Wiesner et al., 2002). Recently, the oscillatory polymerization regime that generates the "hopping" movement of *Listeria* mutants was reconstituted in the motility medium (Bernheim-Grosswasser et al., 2002). The shift in the motility regime from continuous to periodic appeared to be controlled by the size of the beads and the surface density of the activator of Arp2/3.

A chemically controlled medium offers advantages in analyzing the mechanism at work, because the dependence of velocity on the concentration of different factors and their interplay with the surface density of N-WASP can be addressed in a significant concentration range. In the present work, the dependence of the velocity of beads on the density of actin filaments and on the viscous drag is analyzed. Using rhodamine-labeled actin and Alexa®488-labeled Arp2/3 complex in motility assays, insight is obtained into the mechanism by which Arp2/3 complex branches filaments at the bead surface and on the dependence of the frequency of filament branching on the rate of barbed end capping. Evidence is shown for the role of autocatalytic filament branching in the regulation of movement. The results are compared with the behaviors predicted by models based on different mechanistic assumptions (Carlsson, 2001, 2003; Mogilner and Oster, 2003), and their implications in extension of lamellipodia are discussed.

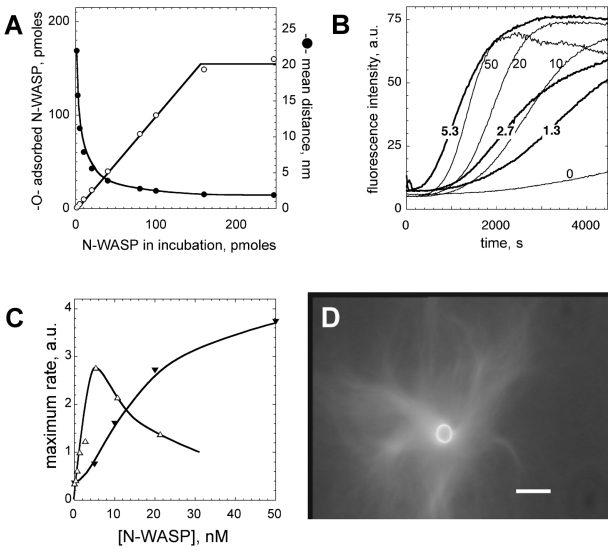

Figure 1. **N-WASP–coated beads stimulate actin polymerization via local activation of Arp2/3 complex.** (A) Characterization of the surface density of N-WASP. Beads of 2 μm diameter (3×10^7 beads) were incubated in 50 μl of buffer C containing the indicated amount of N-WASP (in pmol). The amount of immobilized N-WASP was derived from SDS-PAGE and immunoblots as described in the Materials and methods. Data are represented in terms of a binding isotherm (open circles) or of the average distance between the immobilized N-WASP molecules, calculated as the square root of the reciprocal of the surface density (closed circles). (B) Typical fluorescence polymerization curves of actin (2.5 μM, 10% pyrenyl labeled) in the presence of 25 nM Arp2/3 complex and either soluble N-WASP (thin lines) or immobilized N-WASP (2-μm-diameter beads, thick lines). The number on each curve represents the concentration of N-WASP (in nM), in the case of soluble N-WASP. In the case of immobilized N-WASP, this number represents the concentration that would be obtained if all immobilized molecules were free in solution. (C) Maximum rates of polymerization were measured at half-time of polymerization in a series of assays as shown in B; N-WASP was free in solution (closed triangles) or immobilized on beads (open triangles). The rates are plotted versus the concentration of N-WASP in the assay (as the number of pmol of N-WASP per ml of solution). (D) Actin (2.5 μM) was polymerized in the presence of Arp2/3 complex (25 nM) and 8×10^6/ml N-WASP–coated beads (2 μm diameter). Beads were observed in the microscope after addition of 2.5 μM rhodamine-phalloidine and a 500-fold dilution in microscopy buffer. Bar, 5 μm.

Results

The stimulation of actin assembly and the motility of N-WASP–coated beads depend on the surface density of N-WASP

The adsorption of N-WASP to carboxylated polystyrene beads, as determined by SDS-PAGE and quantitative immunoblot analysis, was linear up to a saturating surface density of 20 N-WASP molecules per 100 nm^2 ($d_s = 0.2$). This corresponds to an average distance of 2 nm between the immobilized N-WASP molecules, consistent with a close packing arrangement (Fig. 1 A). The ability of immobilized N-WASP to activate Arp2/3 complex and stimulate filament branching was assayed in polymerization assays and in motility assays.

Polymerization assays. When immobilized on a bead, N-WASP retained its ability to act as an enzyme that catalyzes branching of actin filaments, thus accelerating actin polymerization as it does in solution (Pantaloni et al., 2000). The stimulation of filament branching by N-WASP–Arp2/3 was one order of magnitude greater when N-WASP was immobilized than when the N-WASP molecules, in identical number, were free in solution. Immobilized N-WASP activated Arp2/3 complex and stimulated actin polymerization constitutively (Fig. 1 B). In contrast to soluble N-WASP, immobilized N-WASP was not further activated by PIP_2. The same stimulation of actin polymerization was achieved when beads were coated with either His-tagged or GST-tagged N-WASP, which, in the soluble state, do not activate Arp2/3 complex to the same extent in the absence of activators like PIP_2 (unpublished data). The stimulation of actin polymerization increased with the density of immobilized N-WASP and reached a maximum followed by a decrease (Fig. 1 C). Maximum stimulation was reached at a calculated average distance of 6 nm between the immobilized N-WASP molecules.

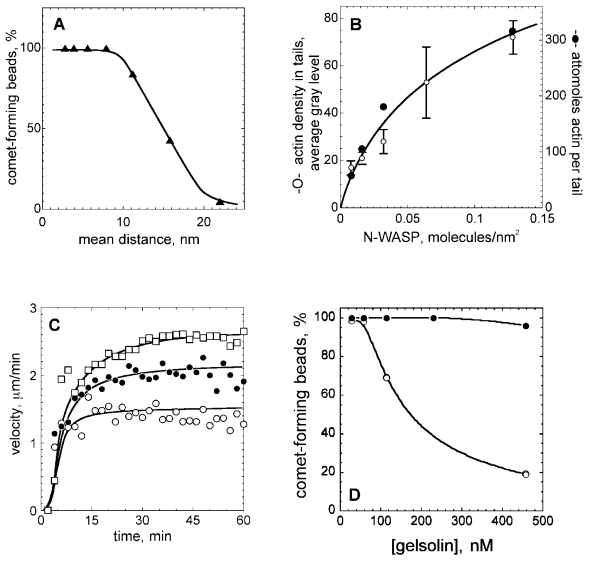

Figure 2. **Influence of the surface density of N-WASP on actin-based motility of N-WASP–coated beads in the motility medium.** (A) Efficient movement requires a minimum surface density of N-WASP. Beads (2 μm in diameter) were coated with different densities of N-WASP, corresponding to the indicated average distance between the adsorbed molecules. The percent of beads that moved with comet tails in the standard motility medium was recorded by phase contrast microscopy after a 1-h incubation. Average values were determined for sets of 100 beads. (B) The density of actin filaments in the actin tail correlates with the surface density of N-WASP. The assay contained 5.5 μM ADF. (B, open circles) The optical density of the actin filaments in the tail attached to beads of 2 μm diameter was measured, as the mean average gray value, in a 2 × 2-μm square placed at a distance of 2 μm from the center of the bead, with two opposite sides of the square arranged parallel to the tail axis (open circles). The optical density of the background is subtracted. (B, closed circles) Evaluation of the amount of actin in tails by sedimentation followed by SDS-PAGE. (C) The steady-state velocity of beads was reached in 10–20 min after addition of beads to the motility medium. Mean velocities of beads (2 μm diameter; d_s = 0.064, 0.13, and 0.016, top to bottom curves) were determined as described, and average mean velocities were calculated from sets of 6–12 beads per coating density. Conditions are the same as in B. (D) The inhibition of movement by an excess of gelsolin is more prominent at a low surface density of N-WASP. The number of motile beads coated with N-WASP at surface densities of 0.008 (open circles) and 0.1 (closed circles) was scored in the motility medium containing the indicated concentrations of gelsolin. A mixture of fluorescent high-density beads and nonfluorescent low-density beads was analyzed in the same sample. After a 45-min incubation in the motility medium, aliquots of the assays were deposited onto slides. Five phase contrast and fluorescence images per assay were immediately taken, and average values for tail formation were determined from overlay images for sets of 20–40 beads per coating type.

The suspension of beads that had initiated actin polymerization in the presence of Arp2/3 was observed in the light microscope after rhodamine-phalloidin staining. Asters of radially arranged filaments were seen around each bead (Fig. 1 D). The symmetry of this pattern was never broken. Many free filaments were also seen in the solution. Because these numerous filaments formed so rapidly, they cannot possibly have arisen from spontaneous actin polymerization, rather they must have been generated by branching at the bead surface and then released in solution. At low N-WASP density, beads holding only a few end-attached filaments were seen, in agreement with previous observations in *Xenopus* egg extracts (Cameron et al., 2001).

Motility assays. The proportion of motile beads (2 μm diameter) forming actin tails in the reconstituted motility medium increased with the surface density of N-WASP above a threshold value corresponding to an average distance of 20 nm between the N-WASP molecules, and reached 100% at an average distance of 8 nm between the immobilized N-WASP molecules (Fig. 2 A). The amount of F-actin in the tails increased with the surface density of N-WASP (Fig. 2 B). The velocity of beads also increased with the surface density of N-WASP and reached a plateau in the range 0.032–0.13 N-WASP/nm^2, corresponding to average distances of 5.6–2.8 nm between the N-WASP molecules. At all surface densities of N-WASP, the steady-state velocity of beads was reached after an ~10-min incubation in the medium and remained constant for >1 h (Fig. 2 C).

The effect of the surface density of N-WASP on motility depended on the concentration of gelsolin (Fig. 2 D). Highly coated beads (d_s = 0.1) all displayed actin tails in the range of 20–400 nM gelsolin. In contrast, at a low density of N-WASP (d_s = 0.007), the percentage of beads that displayed actin tails decreased dramatically upon increasing gelsolin concentration, in a manner similar to the inhibition of *Listeria* or *Shigella* movement by an excess of capping protein (Loisel et al., 1999). In the standard composition of the motility medium (100 nM gelsolin), only 70% of the low-density beads had actin tails. The proportion of beads that showed tails reached 100% at 20 nM gelsolin and decreased to 20% at 400 nM gelsolin. In conclusion, a precise balance between the frequency of filament end branching by surface-activated Arp2/3 complex and end capping by gelsolin is crucial for optimal motility.

Bead velocity is not affected by very large increases in viscosity

To understand the dependence of bead velocity on external load, movement of beads of different diameters in the range of 0.2–3 μm was monitored. At a given surface density of N-WASP, all beads moved at identical rates (Fig. 3 A). Typical trajectories of beads of different sizes in the same field are shown in Fig. 3 B (see also Video 1, available at http://www.jcb.org/cgi/content/full/jcb.200207148/DC1). This result suggests that the velocity is not affected by the load due to the increase in size.

To slow down actin-based propulsion of the beads, the viscosity of the motility medium was increased by the addition of methylcellulose. In contrast to laser trapping, which immobilizes the bead but does not impose a brake to actin assembly, the viscous force that opposes movement is exerted on the ensemble bead + actin tail. To discriminate between the effects of methylcellulose that truly result from the increase in viscosity and those that may arise from properties of methylcellulose independent of viscosity, three kinds of methylcellulose of different polymer length (Sigma-Aldrich catalog nos. M-7140, M-0262, and M-0512, yielding viscosities of 15 cP, 400 cP, and 4,000 cP, respectively, for a 2% concentration wt/vol at 20°C, as compared with 1 cP for standard aqueous buffer) were tested, first on actin polymerization in vitro and then in the motility assay.

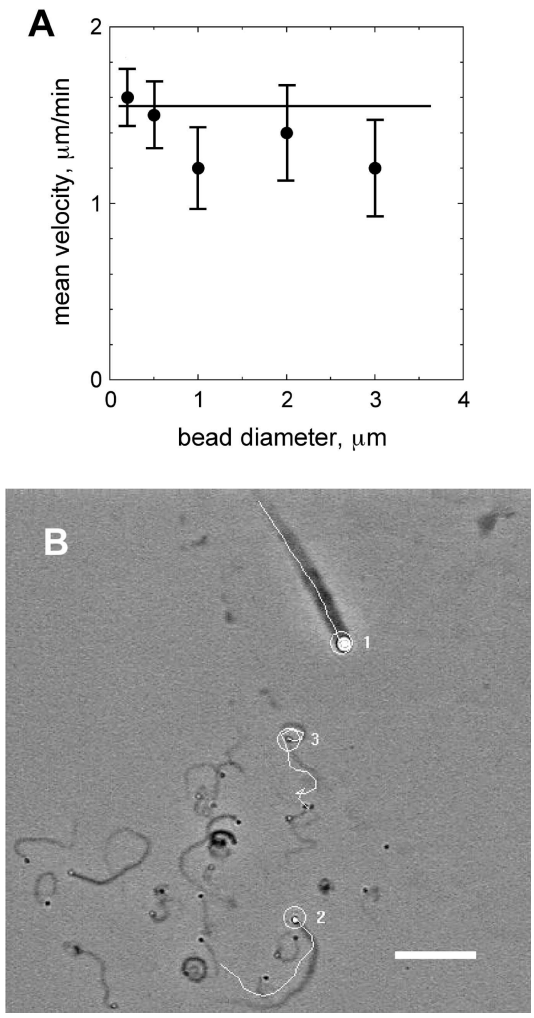

Figure 3. **The velocity of beads is independent of their size.** (A) Beads of different diameters (0.2–3 μm, relative sizes are drawn at the bottom of the panel) were coated with N-WASP (d_s = 0.016). Movement was recorded in the standard motility medium. (B) Trajectories of beads of different diameters (1, 3 μm; 2, 1 μm; 3, 0.5 μm) moving in the same field in the standard motility medium were recorded over a period of 60 min and traced in white on the last frame image (see also Video 1, available at http://www.jcb.org/cgi/content/full/jcb.200207148/DC1). Bar, 15 μm.

The critical concentrations for actin assembly at either the barbed or the pointed end were not affected by up to 2% of any kind of methylcellulose (unpublished data). The kinetics of pyrenyl–actin fluorescence change upon spontaneous actin assembly were not greatly affected by up to 2% methylcellulose of any kind, however spontaneous nucleation was favored by methylcellulose. In addition, the increase in light scattering or turbidity at 350 nm was much larger in the presence of all species of methylcellulose, reflecting bundle formation (Fig. 4 A), in agreement with previous observations (Takiguchi, 1991). Bundling of filaments increased with the concentration but not with the length of the methylcellulose polymer, i.e., it was independent of the viscosity of the solution. Interestingly, at the same mass concentration, methylglucose (monomer of methylcellulose) failed to bundle actin filaments.

To evaluate the drag force exerted on the moving beads according to the Stokes law, viscosity measurements were performed (see Materials and methods). The values of the viscosity derived from the low shear, rheology, and laser tracking microrheology (LTM) measurements were in quantitative agreement, indicating that the Cox-Merz relationship (Haque and Morris, 1993) is verified in the motility medium containing methylcellulose. The presence of 8 μM F-actin in the solutions did not affect the viscoelastic behavior of the medium, which is dominated by methylcellulose.

LTM measurements (Fig. 4 B) yielded the frequency dependence of the viscoelastic modulus G(f) for solutions containing different amounts of methylcellulose. In water, used as a reference, the trapping force of the detection beam affected the power spectrum at low frequencies (up to 30 s^{-1}), causing an apparent increase in G. This effect disappeared in the presence of methylcellulose as the bead motion was dominated by the increasingly viscous medium. No low-frequency plateau was detected, indicating that there was no elastic component in G(f). Assuming that the Stokes law that holds for a purely viscous fluid can be generalized to all frequencies, the solution viscosity is derived using $\eta = G/(2\pi f)$. The characteristic frequency of 2-μm beads propelled at a velocity (v) of 3 μm/min is $f_c = v/(2R) = 0.025\ s^{-1}$. The values of η determined at f_c using the different methods are given in Table I.

Addition of up to 2% of the "long" methylcellulose (M-0512; 4,000 cP at 20°C) failed to slow down actin-based movement of beads, independent of the surface density of N-WASP. In the presence of 4% methylcellulose, the velocity measured using long methylcellulose was only 25% lower than using short methylcellulose (M-7140; 15 cP at 2%). Movement was slower than the one measured at lower concentrations of methylcellulose, however the increase in viscosity was clearly not responsible for the lower velocity. The viscosity of a 4% methylcellulose (M-0512) is too high to be evaluated using the current methods, but an estimate

Table I. **Viscosity measurements of methylcellulose solutions used to slow down actin-based movement of polysterene beads**

	Solution				
	Water	**1% M-7140**	**1% M-0262**	**1% M-0512**	**2% M-0512**
η (Pa · s) (LTM)	4×10^{-3}	9×10^{-3}	0.1	0.7	7.0
η (Pa · s) (low shear)	1×10^{-3}	5×10^{-3}	0.05	0.2	3.3
η (Pa · s) (rheometer)	1×10^{-3}	ND	ND[a]	ND[b]	3.6

Viscosity measurements were performed at 20°C.
[a]A value of 0.08 Pa · s was found for a 0.75% solution.
[b]A value of 0.22 Pa · s was found for a 0.8% solution.

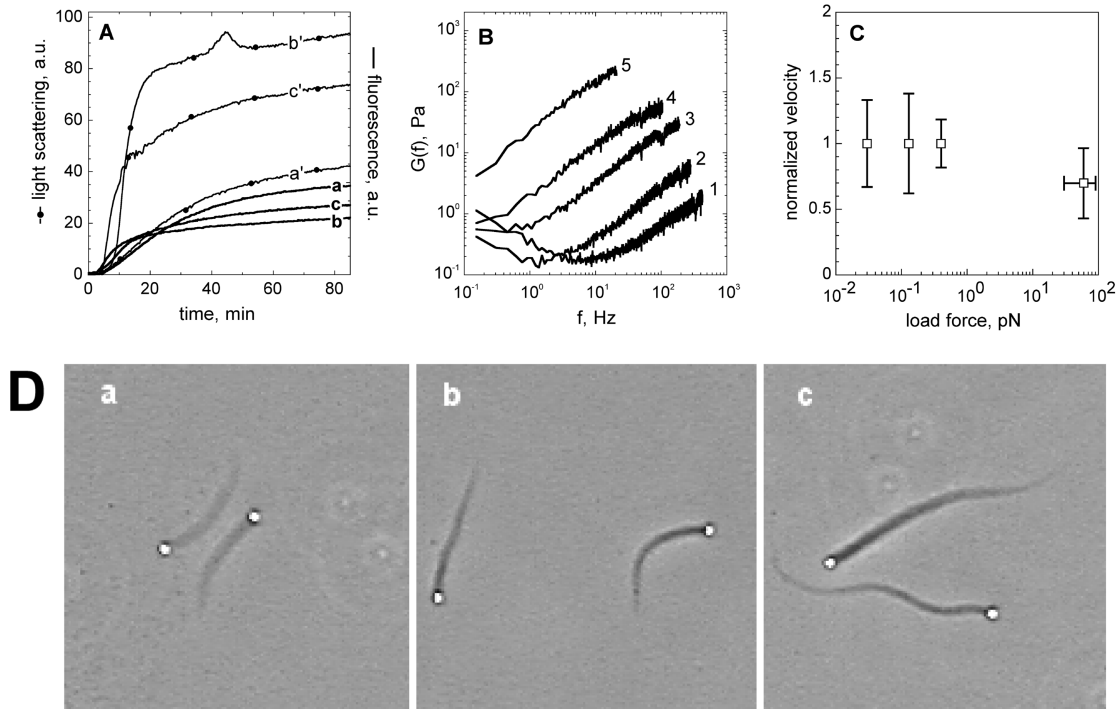

Figure 4. **Effects of methylcellulose on solution viscosity, actin polymerization, and bead movement.** (A) Methylcellulose bundles actin filaments. Polymerization of 4.7 μM actin (10% pyrenyl labeled) was monitored simultaneously by fluorescence (λ_{exc} = 366 nm; λ_{em} = 407 nm) and by light scattering at 90° angle (λ = 350 nm) using a Safas spectrofluorimeter in the absence (a and a′) and in the presence of methylcellulose M-7140 (15 cP at 2%) (b and b′) or M-0512 (4,000 cP at 2%) (c and c′). (B) LTM measurements. The frequency dependence of the viscoelastic modulus G(f) was obtained from the spectral densities, $<\Delta r^2(f)>$, of beads in Brownian motion in different solutions (from bottom to top: water [1], 1% M-7140 [2], 1% M-0262 [3], 1% M-0512 [4], and 2% M-0512 [5]). (C) The force–velocity relationship for actin-based propulsion in increasingly viscous assays is almost flat up to a viscous force of 50 pN. Viscous forces were derived from the Stokes equation using the velocities and viscosities tabulated in Tables I and II, respectively, for increasing concentrations of methylcellulose M-0512. To account for the effect of methylcellulose not related to viscosity, velocities were normalized by dividing by the velocity measured in the presence of the same mass amount of "short" nonviscous methylcellulose. (D) Methylcellulose increases the density of the actin tails in a manner unrelated to the increase in viscous drag. Phase contrast images of N-WASP–coated beads (diameter 2 μm) moving in media containing (a) no methylcellulose, (b) 1% methylcellulose M-7140, and (c) 1% methylcellulose M-0512.

of 10^5 to 3×10^5 cP (100 to 300 Pa · s) can be extrapolated from viscosity measurements made in the range of 0–2% methylcellulose. This represents a 10^5-fold higher viscosity than the aqueous standard motility assay. The corresponding drag force on 2-μm-diameter beads moving at v = 1 μm/min was $F = 6\pi\eta Rv$ = 30–90 pN. In summary, the force–velocity relationship of actin-based movement (Fig. 4 C) has a very low slope in the range of 0–50 pN, indicating that very large forces are developed by site-directed actin assembly. Consistent with this conclusion, recordings of moving beads occasionally show beads that are stuck to the glass coverslip, however the actin tail is pushed backward by actin polymerization at a rate equal to the rate at which neighboring beads move forward (see Video 1). Velocity measurements at different concentrations of methylcellulose are summarized in Table II.

Phase contrast microscopy observation of the moving beads showed that the density of actin filaments in the tail

Table II. **Actin-based velocity in the presence of methylcellulose**

Experiment	Methylcellulose species and concentration						
	M-0512						M-7140
	0%	0.22%	0.45%	0.9%	2%	4%	4%
A		2.4 ± 0.8 (*n* = 14)	2.6 ± 1 (*n* = 7)	2.8 ± 0.5 (*n* = 4)			
B	1.3 ± 0.5 (*n* = 6)				0.73 ± 0.23 (*n* = 10)		
C	3.5 ± 0.6 (*n* = 12)					0.86 ± 0.04 (*n* = 3)	1.2 ± 0.4 (*n* = 6)

Actin-based movement of beads (2 μm in diameter) was monitored in the standard motility medium containing the indicated amounts of different species of methylcellulose. High concentrations of methylcellulose were obtained by adding the required weighed material to the motility medium at 0°C and then bringing the sample to 20°C after solubilization. Velocities are expressed in μm/min.

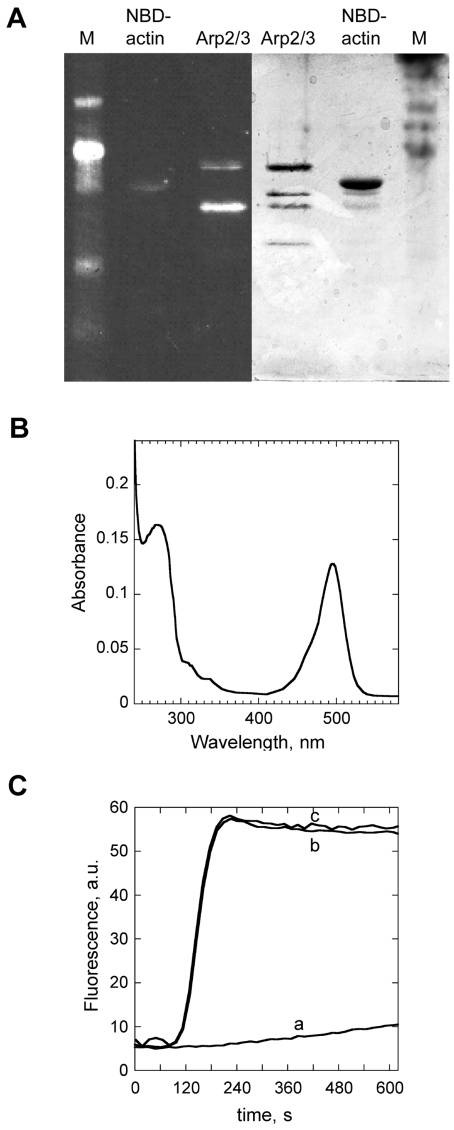

Figure 5. **Fluorescent labeling of Arp2/3 complex.** Arp2/3 complex was labeled with Alexa®488-C5-maleimide as described in the Materials and methods. (A) SDS-PAGE of Alexa®488-labeled Arp2/3 (right, CB staining; left, UV illumination) reveals the incorporation of the label in the p40 subunit (80%) and in Arp3 (20%). M, fluorescent markers. (B) UV-visible spectrum of the labeled Arp2/3 complex. (C) The filament branching activity of Arp2/3 complex is not affected by Alexa®488 labeling. Actin (2.5 μM, 10% pyrenyl labeled) was polymerized in the presence of 0.5 μM VCA, in the absence (a) or presence of 30 nM Arp2/3 before addition (b) and after a 1-h incubation with Alexa®488-C5-maleimide (c).

increased upon addition of methylcellulose, consistent with bundling of filaments in the tails (Fig. 4 D). The average concentration of F-actin in the tail derived from sedimentation measurements was 1 mM in the absence of methylcellulose, similar to the in vivo concentration of F-actin in lamellipodia (Abraham et al., 1999). Comparison of the density of actin tails in the absence and presence of methylcellulose indicated that the concentration of F-actin increased up to 4 mM upon increasing the concentration of methylcellulose to 2%. Again this effect was observed with methylcellulose of different chain length; hence, it was not related to the increase in viscosity and may reflect the change in the activity of water due to methylcellulose.

Arp2/3 complex is incorporated in the actin tail upon barbed end branching of filaments at the surface of the bead

The relationship between velocity and frequency of filament branching during propulsion was examined using rhodamine-labeled actin and Alexa®488-labeled Arp2/3 complex in the motility medium. Several labeling procedures of Arp2/3 complex using a variety of fluorophores were initially tried. The most satisfactory results were obtained using Alexa®488-C5-maleimide (see Materials and methods). Routinely, 3–4 mol of Alexa®488 fluorophore were covalently incorporated per mole of Arp2/3 complex without any loss in filament branching activity. 80% of the label was bound to the ARCp41 subunit, which contains five cysteines (Fig. 5).

Both rhodamine–actin and Alexa®488–Arp2/3 were localized throughout the actin tails. In addition, Alexa®488 fluorescence was intense on the bead, consistent with the tight binding of Arp2/3 to immobilized N-WASP (Fig. 6, A and B). The distribution of the rhodamine and Alexa®488 fluorescence intensities along the tails shows the same exponential decrease for actin and Arp2/3 from the proximal to the distal regions of the tail, suggesting that actin and Arp2/3 complex are lost at identical rates by pointed end depolymerization (Fig. 6 C).

To elucidate whether Arp2/3 simply binds to filaments in the tail or is incorporated in the filaments upon branching at the bead surface, the following experiment was performed. Beads were incubated for 30 min and underwent stationary movement in a motility medium containing unlabeled Arp2/3 at 50 nM. The sample was then supplemented with 50 nM Alexa®488-labeled Arp2/3. To know which form of Arp2/3 (inactive or activated) may potentially interact with the sides of filaments, Alexa®488–Arp2/3 was added either alone or together with VCA (the COOH-terminal domain of N-WASP that constitutively activates Arp2/3). The sample was immediately observed in phase contrast and fluorescence. In the absence of VCA, Arp2/3 fluorescence was initially seen only at the surface of the beads and at the origin of the actin tails, close to the beads, but was absent from the rest of the tail. The gradual increase in Arp2/3 fluorescence in the whole tail took place from the bead surface toward the tail end and kinetically correlated with the movement of beads (Fig. 6, D and E). When both VCA and fluorescently labeled Arp2/3 were added together to the sample, the beads were much less bright than in the absence of VCA, confirming that VCA competes with immobilized N-WASP for binding Arp2/3. However, in spite of the very high local F-actin concentration (1 mM), no fluorescence was detected on the tail, demonstrating that VCA-activated Arp2/3 does not associate with the sides of actin filaments. The addition of VCA eventually caused disruption of the actin tails and arrest of movement. We conclude that neither free Arp2/3 nor VCA-activated Arp2/3 (i.e., the ternary G-actin–VCA–Arp2/3 complex) is able to elicit side branching of filaments. Therefore, the presence of

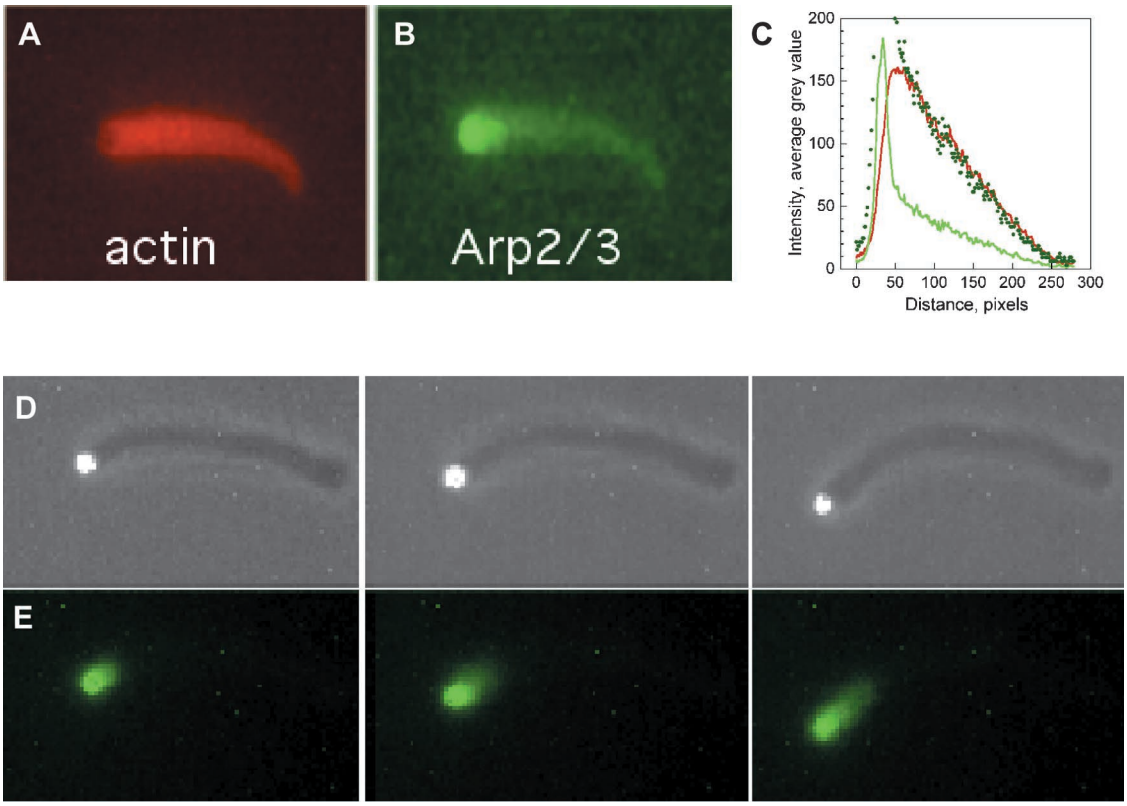

Figure 6. **Arp2/3 complex is incorporated in the actin tail after branching of filaments at the bead surface.** N-WASP–coated beads (2 μm in diameter; d_s = 0.032) were placed in the motility medium containing 2% rhodamine-labeled actin and 100% Alexa®488-labeled Arp2/3. A typical bead and its actin tail are shown in rhodamine fluorescence (A) and Alexa®488 fluorescence (B). The actin/Arp2/3 stoichiometry is constant along the actin tail (C), the figure shows the fluorescences of rhodamine–actin (red curve) and Alexa®488–Arp2/3 (green curve) along an actin tail. Note the sharp peak in the Alexa®488 signal that corresponds to Arp2/3 binding to the bead. Green dotted line is a fourfold expansion of the continuous green curve, emphasizing the identical rhodamine and Alexa®488 decays. Beads in a stationary regime of propulsion in the motility medium containing unlabeled Arp2/3 were supplemented with fluorescent Arp2/3 complex and observed in phase contrast (D) and in Alexa®488 fluorescence (E) at 8, 15, and 22 min after addition of fluorescent Arp2/3. The medium contained 50 nM gelsolin and 1.5 μM ADF, ensuring slow movement (0.4 μm/min) to facilitate measurement of the early steps of Arp2/3 incorporation in the tail.

Arp2/3 complex in the actin tails during movement is solely due to its incorporation in the filaments upon end branching at the surface of the bead. The constant ratio of the densities of actin and Arp2/3 along the tail (Fig. 6 C) therefore demonstrates that the frequency of filament branching is steady during stationary movement.

Computational simulations have indicated that branch spacing (the reciprocal of the frequency of filament branching) provides a means to discriminate between different models (Carlsson, 2001). Bead velocity and average branch spacing were measured at different concentrations of gelsolin in the range of 20–200 nM, using rhodamine-labeled actin and Alexa®488-labeled Arp2/3. The change in actin tail morphology upon increasing gelsolin is visible in phase contrast microscopy (Fig. 7 A). The density of rhodamine-labeled actin in the tail decreased upon increasing gelsolin, reflecting the role of gelsolin in regulating the life time of growing filaments (Pantaloni et al., 2000). On the other hand, the fluorescence ratio of rhodamine–actin to Alexa®–Arp2/3, which is indicative of the branch spacing, decreased upon increasing the capping rate (Fig. 7, B and C). A fourfold higher density of branching was associated with a 10-fold increase in gelsolin concentration. This result suggests that due to the very high density of activated Arp2/3 at the surface of the bead, the competition between Arp2/3 and capping protein for barbed end branching is less effective at the bead surface. The result is consistent with models assuming that barbed end branching occurs at the surface of the bead (Carlsson, 2001). At two different densities of N-WASP, bead velocity displayed a bell-shaped dependence on gelsolin concentration (Fig. 7 D), as previously observed with *Listeria* or *Shigella* (Loisel et al., 1999). This result too is consistent with computational simulations, which predict that velocity should decrease at high capping rates if uncapping does not occur, whereas a constant velocity should be observed if uncapping occurs (Carlsson, 2001).

Discussion

A chemically controlled motility assay has brought insight into the mechanism of actin-based motility. The dependence of movement on the surface density of N-WASP, the external load, and the composition of the medium have been analyzed. The experiments were performed with the goal to compare data with theoretical behaviors predicted by computational simulations using different models (Carlsson, 2001; Mogilner and Oster, 2003). The following conclusions have been reached.

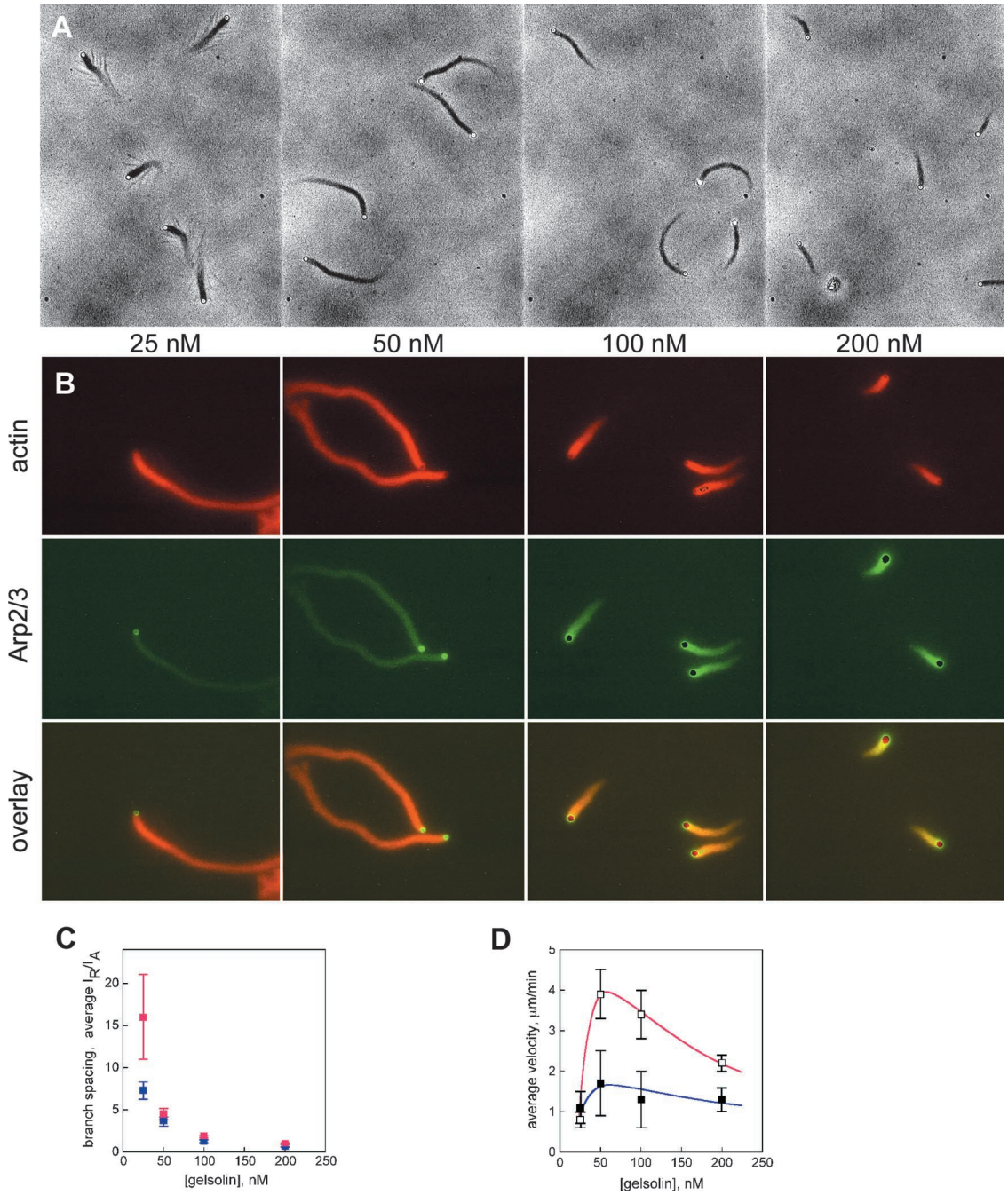

Figure 7. **Evaluation of the branch spacing in actin tails: dependence on gelsolin.** (A) Typical images of tail morphologies for high-density beads (diameter 2 μm) at the indicated gelsolin concentrations. Note the presence of "fishbone" actin tails at low gelsolin, as previously reported (Pantaloni et al., 2000), and the decrease in tail length upon increasing gelsolin. (B) Quantitation of actin (rhodamine labeled) and Arp2/3 (Alexa®488 labeled) in the actin tails at different concentrations of gelsolin. The gallery shows typical images of high-density beads (diameter 2 μm) at indicated gelsolin concentrations. Alexa® fluorescence is saturated on the beads at 100 and 200 nM gelsolin. Note the decrease in the intensities ratio (I_R/I_A) as the gelsolin concentration increases. (C) Branch spacing is a decreasing function of the filament capping rate. Average I_R/I_A ratios were determined for sets of high-density (d_s = 0.064, pink squares) and low-density beads (d_s = 0.016, blue squares) at different gelsolin concentrations. For both bead types, branch spacing decreases sharply upon increasing the gelsolin concentration. (D) Bead velocity shows a bell-shaped dependence on filament capping. Average velocities are shown for high-density (d_s = 0.064, open squares/pink curve) and low-density beads (d_s = 0.016, closed squares/blue curve) at varying gelsolin concentrations.

Force production by actin polymerization and relation between velocity and external load

Increasing the surface density (d_s) of the filament branching enzyme N-WASP on the beads while keeping the composition of the medium constant provided a means to vary the number of filaments pushing the bead. At all values of d_s, velocity reaches a stationary value within 10 min. This steady velocity increases with d_s and then reaches a higher limit in a range of high d_s. These results imply that in the stationary regime, the forces applied to the bead cancel out. Therefore a

force exists that opposes the propulsive force due to actin polymerization. When d_s increases, the number of pushing filaments and the propulsive force increase, tending to accelerate the movement. The fact that a (higher) constant velocity is established indicates that the force opposing propulsion increases too with the number of filaments or with velocity, acting like a drag, and balances the propulsive force. If the force opposing propulsion was the external viscous drag due to the friction of the actin tail against the medium, it could be easily enhanced by increasing the viscosity of the medium. Strikingly, however, a 10^5-fold increase in viscosity fails to slow down movement. This result demonstrates that it is not the external viscous drag that opposes the force resulting from filament growth, but an internal friction force. The fact that external forces up to 50 pN fail to appreciably slow down the beads implies that both the propulsive force and the opposing internal drag must be very large as compared with 50 pN, and must lie in the nN range. Internal friction forces may be due, in part, to the polymerization process itself, e.g., diffusion of G-actin to the filament ends, or to the fact that, as described by Mogilner and Oster (2003), part of the filaments are attached (while branching) whereas others are detached (while growing). In conclusion, large forces can be developed by site-directed actin polymerization.

This view is supported by other observations. For instance, *Listeria* propulsion in *Xenopus* egg extracts could not be arrested by optical tweezers (Gerbal et al., 2000); *Listeria* movement in infected cells is not slowed down by intracellular obstacles nor by the plasma membrane. In the present work, a force sufficient to arrest beads by sticking to the glass surface does not prevent actin from polymerizing and pushing the actin tail backward in a process reminiscent of the retrograde flow in adherent cells, confirming that the power of the actin nanomachine is greater than that of the external viscous drag.

The low slope of the force–velocity relationship in the 0–50 pN range has bearings regarding the molecular mechanism by which filaments are generated by N-WASP–activated Arp2/3 complex. Arp2/3 has been often considered as nucleating filaments from G-actin subunits (Mullins et al., 1998; Higgs and Pollard, 1999). Recent simulations (Carlsson, 2001, 2003; Mogilner and Oster, 2003) show that if filaments are simply nucleated at the surface of the bead, the velocity is predicted to drop rapidly upon application of forces as low as 10 pN, whereas a much slower decay is predicted by a model in which filaments are created by autocatalytic branching (Carlsson, 2001, 2003). Our data fully support the autocatalytic filament branching function of Arp2/3.

Our data and conclusions differ on two points from a recent report showing that addition of 1% methylcellulose caused a 20-fold decrease in the velocity of *Listeria* in *Xenopus* egg extracts (McGrath et al., 2003). First, the nominal viscosity of the methylcellulose (M-0262; Sigma-Aldrich) used by the authors is 10-fold lower than that of the methylcellulose (M-0512; Sigma-Aldrich) used here to slow down the beads; yet at a concentration of 1%, it did appreciably slow down bacteria in cell extracts. Second, the viscous drag was evaluated to ~200 pN at 1% methylcellulose, when bacteria moved at 0.1 μm/min, implying that the viscosity around the bacteria would have been at the order of 10^3 Pa · s, i.e., 10^4-fold higher than the nominal value.

Several reasons may account for the differences between the two works. First, the present reconstituted medium supports motility in a more efficient fashion than diluted *Xenopus* egg extracts. Actually, wild-type *Listeria* fail to move in *Xenopus* egg extracts, whereas they move as well in the reconstituted medium as in vivo (Boujemaa-Paterski et al., 2001). Only a fraction of *Listeria* overexpressing ActA are generally able to move in *Xenopus* egg extracts, whereas 100% of the beads and bacteria move in the motility medium. Second, friction of bacteria against the glass surface of the chamber (McGrath et al., 2003) may have added to the viscous drag, explaining the apparent discrepancy between the measured and nominal viscosities. Wall effects may be less prominent in our experiments, due to the use of 10-μm-deep chambers. Third, methylcellulose may affect viscosity differently in buffer and in cell extracts.

Arp2/3 incorporates in filaments after barbed end branching at the bead surface

The use of double fluorescent labeling of actin and Arp2/3 in motility assays enlightens the Arp2/3 mechanism. Arp2/3 complex incorporates in the actin tail in an endwise fashion from the surface of the beads toward the core of the tail. Both Arp2/3 and actin densities decrease along the tail, while keeping in a constant ratio. If Arp2/3 dissociated from the filaments upon debranching, the ratio of Arp2/3 to actin would be lower at the distal end of the tail than close to the bead. The observed opposite result suggests that Arp2/3 remains bound to the mother branch after debranching and is released from the tail upon filament depolymerization.

In spite of the very high local concentration of F-actin (1 mM) in the tail, Arp2/3 complex, either free or activated, in complex with VCA, does not readily bind to the sides of filaments in the tail. It is only upon barbed end branching that Arp2/3 complex becomes associated with filaments and remains in the tail after debranching.

It has been proposed that filament branching could occur by preferential association of activated Arp2/3 complex with the sides of F-actin subunits close to the barbed end, implying that Arp2/3 complex would bind preferentially to ADP–P*-actin or ATP–F-actin (Cooper et al., 2001; Ichetovkin et al., 2002). This view, which would account for the reported equal length of mother and daughter branches (Pantaloni et al., 2000; Ichetovkin et al., 2002), is in fact not consistent with data (Higgs and Pollard, 1999; Pantaloni et al., 2000; Ichetovkin et al., 2002) showing that side branching is not enhanced in the presence of BeF_3^-, a structural analogue of Pi that reconstitutes the transition state of ATP hydrolysis on F-actin (Combeau and Carlier, 1988). Independently, a recent report (Falet et al., 2002) confirmed that filament barbed ends are required for Arp2/3 complex to be able to branch filaments and that filament branching by Arp2/3 is independent of the F-actin–bound nucleotide.

Velocity is controlled by a balance between autocatalytic filament end branching and capping

Actin-based movement is thus controlled by a balance between filament end branching and capping, as predicted by recent models (Carlsson, 2001) based on our biochemical studies (Pantaloni et al., 2000; Boujemaa-Paterski et al., 2001).

At a given frequency of branching (determined by the surface density of N-WASP and concentration of Arp2/3 in the medium) and at a given steady-state concentration of G-actin, the velocity of beads decreases steeply upon increasing the concentration of gelsolin. According to recent simulations (Carlsson, 2001), this result excludes models in which uncapping occurs, which generate gelsolin-independent velocities, and favors models in which filaments branch from their end.

Double label experiments (with fluorescent actin and Arp2/3) allow us to quantitate branch spacing as a function of gelsolin. In the present simple reconstituted system, the actin arrays are poorly branched at low gelsolin and highly branched at high gelsolin. First, this result is consistent with the modeled behavior within autocatalytic branching. Second, the result offers a possible testable explanation for the different morphologies of actin arrays in lamellipodia and filopodia, which are thought both to be induced by Arp2/3 complex. A high concentration of capping protein may generate the highly branched Arp2/3-rich array in lamellipodia; a low concentration of capping protein in filopodia may generate sparsely branched filaments that easily align in parallel bundles in which Arp2/3 is below the detection limit.

In summary, motility assays have brought insight into how filaments are generated by Arp2/3 complex in motile processes. The different putative mechanisms of action of Arp2/3 complex have important implications in models for lamellipodium extension. Arp2/3 complex has been proposed to nucleate filaments (Mullins et al., 1998; Higgs and Pollard, 1999; Mogilner and Oster, 2003, for modeling studies), bind to the sides of existing filaments in association with a cytoplasmic activator to initiate lateral branches in filaments throughout lamellipodia (Higgs and Pollard, 1999, 2001), or interact, at the membrane, with the barbed end of a filament to initiate the formation of a daughter branch, thus autocatalytically generating a polarized arborescent fractal structure (Pantaloni et al., 2000, 2001; Boujemaa-Paterski et al., 2001). The filament nucleation model is not favored by the observed insensitivity of velocity to viscous drag up to at least 50 pN; the autocatalytic barbed end branching model uniquely accounts for the connection between signaling and force production by barbed end generation and growth.

Materials and methods

Proteins

Actin was purified from rabbit muscle and pyrenyl labeled according to usual procedures (Egile et al., 1999). Human His-tagged N-WASP was expressed in Sf9 cells using the baculovirus system (Egile et al., 1999). Recombinant human ADF was expressed in *Escherichia coli* (Ressad et al., 1998). Profilin was purified from bovine spleen (Pantaloni and Carlier, 1993). Gelsolin from human plasma was a gift from Yukio Doi (Kyoto University, Kyoto, Japan). Arp2/3 complex was purified from bovine brain (Egile et al., 1999). Actin was rhodamine labeled (Isambert et al., 1995). Arp2/3 complex was fluorescently labeled by incubation for 1 h at 0°C with 100 μM Alexa®488-C5-maleimide (Molecular Probes) in 20 mM Hepes, pH 7.2, containing 0.2 mM $MgCl_2$ and 0.2 mM ATP, followed by addition of 1 mM DTT and gel filtration (NAP10; Amersham Biosciences). Four molecules of Alexa®488 fluorophores were covalently bound to Arp2/3, without alteration of the activity of Arp2/3 complex in branching filaments and supporting actin-based motility.

Motility medium

The standard motility medium consisted of a solution of 7 μM F-actin in buffer C (10 mM Hepes, pH 7.8, 0.1 M KCl, 1 mM $MgCl_2$, 1 mM ATP, 0.1 mM $CaCl_2$), supplemented with 3.5 μM ADF, 2.4 μM profilin, 100 nM gelsolin, and 100 nM Arp2/3 complex. As auxiliary agents, the assay contained 5 mg/ml BSA, 0.2% (wt/vol) methylcellulose (yielding a viscosity of 4,000 cP at 2% wt/vol; M-0512; Sigma-Aldrich), 7 mM DTT, and 1.5 mM DABCO (Loisel et al., 1999). Variations in the composition of the standard medium are indicated in the text.

Functionalization of polystyrene beads

Polystyrene carboxylated beads of diameters from 0.2 to 3 μm (Polysciences) were incubated for 1 h on ice in buffer C containing N-WASP. The amount of beads in a 50-μl suspension was adjusted so that the total surface of solid per unit volume of solution was 7.5×10^9 μm^2/ml, independent of the diameter of the beads. BSA (10 mg/ml) was added to block free adsorption sites for another 15 min. The beads were sedimented, washed twice with 250 μl buffer C, and resuspended in 50 μl buffer C containing 1 mg/ml BSA. To account for the loss (typically ~20%) of beads during the functionalization/washing steps, a correction factor was determined for each preparation by measuring the light scattering at 750 nm against standards prepared with the bead stock solution. Functionalized beads were stored on ice and used for up to 1 wk without any change in their motile properties. All experiments shown were performed with freshly coated beads (aged at most 2 d).

The surface capacity of the beads for N-WASP was evaluated by SDS-PAGE analysis of nonbound N-WASP in the supernatants of beads preincubated with N-WASP. Additionally, washed beads were heat denatured in SDS and the amount of adsorbed protein was determined by immunoblotting using an anti–N-WASP polyclonal antibody and comparison with standards. Gel and blot patterns were scanned with an Arcus scanner and analyzed using NIH Image software. The surface density of immobilized N-WASP (d_s, in molecules per nm^2) was derived.

Fluorescence polymerization assay using N-WASP–coated beads, Arp2/3 complex, and pyrenyl-labeled actin

The stimulation of actin polymerization via activation of Arp2/3 complex by N-WASP–coated beads was assayed as follows. Beads (8×10^6 beads/ml) carrying different surface densities of N-WASP were placed in a solution containing 2.5 μM G-actin (10% pyrenyl labeled) and 20 nM Arp2/3 complex. The contribution of light scattering coming from the beads, at this concentration, did not detectably interfere with the fluorescence signal. The time course of polymerization was monitored using the change in fluorescence of pyrenyl-labeled actin.

Motility assay and data analysis

Single assays. Functionalized beads were diluted 50-fold in the motility medium. Depending on the amounts of ADF and/or gelsolin present in the medium, samples (25 μl) were preincubated 5–60 min at room temperature to reach steady state. An aliquot of 2.5 μl was placed between a slide (Superfrost Plus; Menzel-Gläser, GmbH) and a coverslip, sealed with Valap (vaselin, lanolin, paraffin 1:1:1), and observed in phase contrast with a Nikon Diaphot microscope using a CCD camera (Panasonic) and the NIH Image software.

High-throughput assays. Synchronous time-resolved data on several assays were obtained using flow chambers constructed as follows. A series of four to five adjacent 5-mm-wide channels were made by drawing parallel lines across the slide with a hydrophobic marker pen (DakoCytomation). One half of a 40 × 22-mm coverslip (Knittel Gläser) was pressed across these lines, producing four to five flow chambers containing ~1 μl solution each. The chambers were filled by capillarity and sealed with Valap. Synchronous films of up to four selected fields per chamber were recorded with a CCD camera on an Olympus AX70 microscope equipped with a motorized stage (Märzhäuser) using MetaMorph 4.6 for microscope control and image acquisition. A 20× phase objective (NA 0.5) was used, if not indicated otherwise.

Data analysis. Average rates of movement were determined by selecting freely moving beads from at least two different fields of motility assay recordings. For beads of 0.5 μm diameter and larger, the template recognition-based tracking tool of MetaMorph was used to measure mean velocities. For 0.2-μm beads, trajectories were manually retraced and the mean velocity calculated by dividing the trace length by the observation time interval. Average mean velocities were calculated for sets of 5 to 10 beads per assay.

Quantitation of actin and Arp2/3 in the actin tails

Two methods were used to determine F-actin and Arp2/3 densities in the actin tails. First, rhodamine-labeled actin and Alexa®488-labeled Arp2/3 were used in the motility assays, and their respective fluorescence intensi-

ties were recorded with a LHESA 72LL CCD camera using appropriate filters and a 100× objective (NA 1.35). The extent of labeling of Arp2/3 (100%) and of actin (10%) was chosen to yield intensities in the linear response range of the camera for both fluorophores. Control experiments were performed to make sure that no emission overlap existed between the two fluorophores. Images of comets were recorded at steady state, and average emission intensities of rhodamine (I_R) and Alexa®488 (I_A) were measured as mean gray values in a square section of the actin tail at least one bead diameter behind the bead. These values were corrected for dark current and, where necessary, for background fluorescence; an average I_R/I_A ratio was determined from sets of at least five beads. To estimate the absolute stoichiometry of actin and Arp2/3 from these values, a calibration was performed using solutions of the two fluorescent proteins at different concentrations. Second, beads together with their actin tails were sedimented after steady-state establishment at 13,000 *g* for 10 min in an Eppendorf centrifuge. It was verified that the F-actin present in the motility medium did not sediment at all under these conditions. The amount of F-actin in the tails associated with the beads was determined by SDS-PAGE of the pellet followed by Coomassie blue staining and comparison with actin standards.

Viscosity measurements

The drag force (F) exerted by the environment on a sphere in motion is derived from the solution viscosity (η) using the Stokes law: $F = 6\pi\eta Rv$, where R and v are the radius and the velocity, respectively, of the bead. The viscosity of the motility medium was increased by addition of methylcellulose. The following techniques were used to determine the viscosity of the solutions.

Low shear viscosimetry measurements were performed at 20°C in a Contraves LS-30 viscometer. Rheology measurements were performed using a Haake rotation rheometer. The viscosity was derived from the values of the dynamic visco-elastic modulus G*, measured in a frequency range of 10^{-2}–10^{2} s^{-1}.

Unlike the former methods, LTM is a passive technique in which the Brownian thermal motion of particles embedded in a solution is monitored without deforming the materials mechanically (Mason and Weitz, 1995). The viscoelastic properties of the solution are derived from the position fluctuations of the particles.

LTM measurements

Setup. The setup of LTM was implemented on a microscope (Polyvar; Reichert-Jung) as previously described (Helfer et al., 2001). A collimated laser beam (laser diode at 635 nm; HL6320G; Sanyo) enters the microscope and is focused by the microscope objective (oil, ×100, NA 1.32) in the sample. Beads were slightly trapped by the laser beam and thus were centered in the beam focus. The light backscattered from the bead was relayed via the objective and additional lenses to a four-quadrants photodiode (SPOT 4D; UDT) connected to two amplifiers (301-DIV-30KHz; UDT) that deliver signals proportional to the real position of the bead in the focal plane of the objective. The bead motion in time, r(t), was analyzed to compute the power spectrum of the position fluctuations in frequency, $<\Delta r^2(f)>$, using a software written under Labview (National Instruments).

Measurement of the viscoelastic modulus. Polystyrene particles (1 μm in diameter; Polysciences) were used to analyze the different solutions. The motility medium was assumed to be a viscoelastic continuum around the rigid spherical particle. The viscoelastic modulus G(f) was derived from the power spectrum as follows (Mason et al., 1997):

$$G(f) = \frac{k_B T}{2\pi^2 R f \langle \Delta r^2(f) \rangle}.$$

Online supplemental material

Online supplemental material is available at http://www.jcb.org/cgi/content/full/jcb.200207148/DC1. Video 1 accompanies Fig. 3 B. Note that one of the large beads gets immobilized during the sequence; its comet continues to grow at a constant rate.

We thank François Lequeux for a helpful discussion. We thank Scot Kuo, Anders Carlsson, Alex Mogilner, and George Oster for communicating unpublished work.

We gratefully acknowledge financial support from the Ligue Nationale Contre le Cancer (special "Ligue" label to M.-F. Carlier).

Submitted: 26 July 2002
Revised: 18 December 2002
Accepted: 18 December 2002

References

Abraham, V.C., V. Krishnamurthi, D. Lansing Taylor, and F. Lanni. 1999. The actin-based nanomachine at the leading edge of migrating cells. *Biophys. J.* 77:1721–1732.

Bernheim-Grosswasser, A., S. Wiesner, R.M. Golsteyn, M.-F. Carlier, and C. Sykes. 2002. The dynamics of actin-based motility depends on surface parameters. *Nature.* 417:308–311.

Borisy, G.G., and T.M. Svitkina. 2000. Actin machinery: pushing the envelope. *Curr. Opin. Cell Biol.* 12:104–112.

Boujemaa-Paterski, R., E. Gouin, G. Hansen, S. Samarin, C. Le Clainche, D. Didry, P. Dehoux, P. Cossart, C. Kocks, M.-F. Carlier, and D. Pantaloni. 2001. *Listeria* protein ActA mimics WASp family proteins: it activates filament barbed end branching by Arp2/3 complex. *Biochemistry.* 40:11390–11404.

Cameron, L.A., M.J. Footer, A. van Oudenaarden, and J.A. Theriot. 1999. Motility of ActA protein-coated microspheres driven by actin polymerization. *Proc. Natl. Acad. Sci. USA.* 96:4908–4913.

Cameron, L.A., P.A. Giardini, F.S. Soo, and J.A. Theriot. 2000. Secrets of actin-based motility revealed by a bacterial pathogen. *Nat. Rev. Mol. Cell Biol.* 1:110–119.

Cameron, L.A., T.M. Svitkina, D. Vignjevic, J.A. Theriot, and G.G. Borisy. 2001. Dendritic organization of actin comet tails. *Curr. Biol.* 11:130–135.

Carlsson, A.E. 2001. Growth of branched actin networks against obstacles. *Biophys. J.* 81:1907–1923.

Carlsson, A.E. 2003. Growth velocities of branched actin networks. *Biophys. J.* In press.

Combeau, C., and M.-F. Carlier. 1988. Probing the mechanism of ATP hydrolysis on F-actin using vanadate and the structural analogs of phosphate BeF-3 and A1F-4. *J. Biol. Chem.* 263:17429–17436.

Cooper, J.A., M.A. Wear, and A.M. Weaver. 2001. Arp2/3 complex: advances on the inner workings of a molecular machine. *Cell.* 107:703–705.

Egile, C., T.P. Loisel, V. Laurent, R. Li, D. Pantaloni, P.J. Sansonetti, and M.-F. Carlier. 1999. Activation of the Cdc42 effector N-WASP by the *Shigella flexneri* IcsA protein promotes actin nucleation by Arp2/3 complex and bacterial actin-based motility. *J. Cell Biol.* 146:1319–1332.

Falet, H., K.M. Hoffmeister, R. Neujahr, J.E. Italiano Jr., T.P. Stossel, F.S. Southwick, and J.H. Hartwig. 2002. Importance of free filament barbed ends for Arp2/3 complex function in platelets and fibroblasts. *Proc. Natl. Acad. Sci. USA.* 99:16782–16787.

Gerbal, F., V. Laurent, A. Ott, M.-F. Carlier, P. Chaikin, and J. Prost. 2000. Measurement of the elasticity of the actin tail of *Listeria monocytogenes*. *Eur. Biophys. J.* 29:134–140.

Haque, A., and E.R. Morris. 1993. Thermogelation of methyl cellulose. I. Molecular structures and processes. *Carbohydrate Polymers.* 22:161–173.

Helfer, E., S. Harlepp, L. Bourdieu, J. Robert, F.C. MacKintosh, and D. Chatenay. 2001. Viscoelastic properties of actin-coated membranes. *Phys. Rev. E. Stat. Phys. Plasmas Fluids Relat. Interdiscip. Topics.* 63:021904.

Higgs, H.N., and T.D. Pollard. 1999. Regulation of actin polymerization by Arp2/3 complex and WASp/Scar proteins. *J. Biol. Chem.* 274:32531–32534.

Higgs, H.N., and T.D. Pollard. 2001. Regulation of actin filament network formation through ARP2/3 complex: activation by a diverse array of proteins. *Annu. Rev. Biochem.* 70:649–676.

Ichetovkin, I., W. Grant, and J. Condeelis. 2002. Cofilin produces newly polymerized actin filaments that are preferred for dendritic nucleation by the Arp2/3 complex. *Curr. Biol.* 12:79–84.

Isambert, H., P. Venier, A.C. Maggs, A. Fattoum, R. Kassab, D. Pantaloni, and M.-F. Carlier. 1995. Flexibility of actin filaments derived from thermal fluctuations. Effect of bound nucleotide, phalloidin, and muscle regulatory proteins. *J. Biol. Chem.* 270:11437–11444.

Loisel, T.P., R. Boujemaa, D. Pantaloni, and M.-F. Carlier. 1999. Reconstitution of actin-based motility of *Listeria* and *Shigella* using pure proteins. *Nature.* 401:613–616.

Machesky, L.M., and R.H. Insall. 1998. Scar1 and the related Wiskott-Aldrich syndrome protein, WASP, regulate the actin cytoskeleton through the Arp2/3 complex. *Curr. Biol.* 8:1347–1356.

Mason, T.G., and D.A. Weitz. 1995. Optical measurements of frequency-dependent linear viscoelastic moduli of complex fluids. *Phys. Rev. Lett.* 74:1250–1253.

Mason, T.G., K. Ganesan, J.H. van Zanten, D. Wirtz, and S. Kuo. 1997. Particle tracking microrheology of complex fluids. *Phys. Rev. Lett.* 79:3282–3285.

McGrath, J.L., N.J. Eungdamrong, C.I. Fisher, F. Peng, L. Mahadevan, T.J. Mitchison, and S.C. Kuo. 2003. The force-velocity relationship for the actin-based motility of *Listeria monocytogenes*. *Curr. Biol.* In press.

Mitchison, T.J., and L.P. Cramer. 1996. Actin-based cell motility and cell locomotion. *Cell.* 84:371–379.

Mogilner, A., and G. Oster. 2003. Force generation by actin polymerization II: the elastic ratchet and tethered filaments. *Biophys. J.* In press.

Mullins, R.D., J.A. Heuser, and T.D. Pollard. 1998. The interaction of Arp2/3 complex with actin: nucleation, high affinity pointed end capping, and formation of branching networks of filaments. *Proc. Natl. Acad. Sci. USA.* 95: 6181–6186.

Noireaux, V., R.M. Golsteyn, E. Friederich, J. Prost, C. Antony, D. Louvard, and C. Sykes. 2000. Growing an actin gel on spherical surfaces. *Biophys. J.* 78: 1643–1654.

Pantaloni, D., and M.-F. Carlier. 1993. How profilin promotes actin filament assembly in the presence of thymosin β4. *Cell.* 75:1007–1014.

Pantaloni, D., R. Boujemaa, D. Didry, P. Gounon, and M.-F. Carlier. 2000. The Arp2/3 complex branches filament barbed ends: functional antagonism with capping proteins. *Nat. Cell Biol.* 2:385–391.

Pantaloni, D., C. Le Clainche, and M.-F. Carlier. 2001. Mechanism of actin-based motility. *Science.* 292:1502–1506.

Ressad, F., D. Didry, G.X. Xia, Y. Hong, N.H. Chua, D. Pantaloni, and M.-F. Carlier. 1998. Kinetic analysis of the interaction of actin-depolymerizing factor (ADF)/cofilin with G- and F-actins. Comparison of plant and human ADFs and effect of phosphorylation. *J. Biol. Chem.* 273:20894–20902.

Skoble, J., D.A. Portnoy, and M.D. Welch. 2000. Three regions within ActA promote Arp2/3 complex–mediated actin nucleation and *Listeria monocytogenes* motility. *J. Cell Biol.* 150:527–538.

Takiguchi, K. 1991. Heavy meromyosin induces sliding movements between antiparallel actin filaments. *J. Biochem. (Tokyo).* 109:520–527.

Welch, M.D., J. Rosenblatt, J. Skoble, D.A. Portnoy, and T.J. Mitchison. 1998. Interaction of human Arp2/3 complex and the *Listeria monocytogenes* ActA protein in actin filament nucleation. *Science.* 281:105–108.

Wiesner, S., R. Boujemaa, and M.-F. Carlier. 2002. Actin-based motility of *Listeria monocytogenes* and *Shigella flexneri*. *Methods in Microbiology.* 31:245–262.